1   **Night-time chemistry of biomass burning emissions in urban areas: A dual mobile chamber**

2   **study**

3   Spiro D. Jorga[1], Kalliopi Florou[2], Christos Kaltsonoudis[2], John K. Kodros[2], Christina

4   Vasilakopoulou[2,3], Manuela Cirtog[5], Axel Fouqueau[6], Bénédicte Picquet-Varrault[5], Athanasios

5   Nenes[2,4], and Spyros N. Pandis[1,2,3]

6   [1]Department of Chemical Engineering, Carnegie Mellon University, Pittsburgh, 15213, USA

7   [2]Institute of Chemical Engineering Sciences, ICE-HT, Patras, 26504, Greece

8   [3]Department of Chemical Engineering, University of Patras, Patras, 26504, Greece

9   [4]School of Architecture, Civil & Environmental Engineering, Ecole Polytechnique Federale de Lausanne,

10   Lausanne, 1015, Switzerland

11   [5]LISA, UMR CNRS 7583, Université Paris-Est Créteil, Université de Paris, Institut Pierre Simon Laplace

12   (IPSL), Créteil, France

13   [6]Laboratoire National de Métrologie et d'Essais (LNE), 75015 Paris, France

14   *Correspondence to:* Spyros N. Pandis (spyros@chemeng.upatras.gr)

16   **Abstract.**

17   Residential biomass burning for heating purposes is an important source of air pollutants during

18   winter. Here we test the hypothesis that significant secondary organic aerosol production can take

19   place even during winter nights through oxidation of the emitted organic vapors by the nitrate

20   (NO_3) radical produced during the reaction of ozone and nitrogen oxides. We use a mobile dual

21   smog chamber system which allows the study of chemical aging of ambient air against a control

22   reference. Ambient urban air sampled during a wintertime campaign during night-time periods

23   with high concentrations of biomass burning organic aerosol was used as the starting point of the

24   aging experiments. Ozone was added in the perturbed chamber to simulate mixing with

25   background air (and subsequent NO_3 radical production and aging), while the second chamber was

26   used as a reference. Following the injection of ozone rapid organic aerosol (OA) formation was

27   observed in all experiments leading to increases of the OA concentration by 20-70%. The oxygen-

28   to-carbon ratio of the OA increased on average by 50% and the mass spectra of the produced OA

29   was quite similar to the oxidized OA mass spectra reported during winter in urban areas. Further,

30   good correlation was found for the OA mass spectra between the ambient-derived emissions in

31   this study and the nocturnal aged laboratory-derived biomass burning emissions from previous

32   work. Concentrations of NO_3 radicals as high as 25 ppt were measured in the perturbed chamber

33   with an accompanying production of 0.1-3.2 µg m^{-3} of organic nitrate in the aerosol phase. These

34   results strongly indicate that the OA in biomass burning plumes can chemically evolve rapidly

35   even during wintertime periods with low photochemical activity.

36

37   **1 Introduction**

38   Biomass burning from residential heating, agricultural fires, prescribed burning, and

39   wildfires is a major source of atmospheric pollutants worldwide (Watson 2002, Bond et al. 2004,

40   Robinson et al. 2006). Emissions from biomass burning contribute both primary organic aerosol

41   (POA) and organic vapors that upon further reactions in the atmosphere can produce secondary

42   organic aerosol (SOA) (Andreae & Merlet 2001, Akagi et al., 2011, Bruns et al., 2016, Akherati

43   et al., 2020). The use of wood burning for domestic heating purposes is one of the major sources

44   of OA in many countries and is a major contributor to the violation of daily PM standards in

45   European cities (Alfarra et al., 2007, Favez et al., 2010, Fuller et al., 2014). Biomass burning

46   emissions and their products have significant but still uncertain impacts on human health and

47   climate (Ford et al., 2018; O'Dell et al., 2019).

48   The organic aerosol emitted during biomass burning undergoes extensive physical and

49   chemical changes in the atmosphere. More volatile components evaporate as emissions dilute in

50   the atmosphere (Tkacik et al., 2017); these semivolatile organic compounds (SVOCs) together

51   with the other emitted intermediate volatility (IVOCs) and volatile organic compounds (VOCs)

52   are subsequently oxidized leading to the production of SOA. Photochemical oxidation of biomass

53   burning emissions and the resulting SOA production have been studied both in the laboratory

54   (Hennigan et al., 2011; Ortega et al., 2013; Tkacik et al., 2017; Ahern et al.; 2019; Kodros et al.,

55   2020) and in the field (Capes et al., 2008; Jolleys et al., 2015; Vakkari et al., 2018). The reactions

56   of VOCs, IVOCs and SVOCs with the OH radical are considered to be the dominant chemical

57   pathway for oxidation, but reactions of emitted monoterpenes with ozone can also contribute (Yu

58   et al., 1999, Zhao et al., 2015). Despite considerable uncertainties remaining on the amount of

59   SOA that can be produced, and the net change of the biomass burning OA concentration when

60   evaporation is considered, it is clear that this daytime processing is important for converting the

61   fresh biomass burning OA to oxidized OA (OOA) (Bougiatioti et al., 2014).

62   Atmospheric processing of biomass burning OA during periods of low photochemical

63   activity (such as in winter or at night), known also as "dark" aging, has received substantially less

attention than photochemical processing. Recent aircraft measurements during agricultural biomass burning periods indicated that nighttime oxidation of biomass burning VOCs is dominated by NO_3 (Decker et al., 2019). Hartikainen et al. (2018) reported high amounts of nitrogen-containing organic compounds both in the gas and particle phase after dark aging of residential wood combustion emissions. Kodros et al. (2020) reported significant and rapid OOA production in laboratory experiments in which fresh biomass burning emissions were exposed to NO_3 and suggested that dark oxidation may be an important process on regional scales. In the same study, ambient measurements in an urban area suggested that the mixing of O_3 from the residual layer down to the nocturnal boundary layer can enhance the formation of NO_3 and the nighttime oxidation of biomass burning emissions. The mixing of ozone from the residual layer and the importance to nightime chemistry was also suggested in studies on nightime oxidation of biogenic VOCs (Brown et al., 2009; Brown et al., 2013). Despite this important finding, the degree to which biomass burning plumes undergo night-time aging and produce significant amounts of SOA remains poorly understood. Lacking consideration of such nocturnal chemistry in transport models has been suggested as a possible source of the under prediction oxidized organic aerosol mass by a factor of 3-5 (Fountoukis et al., 2016; Tsimpidi et al., 2014) during wintertime in polluted areas with low photochemical activity.

In this study, we take advantage of the high levels of OA from residential biomass burning in Patras, Greece (the country's third-largest city), to investigate the importance of night-time chemistry in the processing of biomass burning OA. Biomass burning leads to concentrations of OA exceeding 50 μg m^{-3} in Patras in the early evening (Florou et al., 2017). A dual atmospheric simulation chamber system is used to elucidate the formation of SOA during winter periods in urban areas with high biomass burning organic aerosol concentrations. Usually chamber studies use fresh biomass burning emissions generated in the laboratory. The use of the dual chamber system offers the capability of aging realistic biomass burning emissions mixed with other pollutants. It therefore offers a bridge between laboratory experiments and ambient observations.

2 Experimental Methods

2.1 Dual chamber system

The dual chamber system developed by Kaltsonoudis et al. (2019) was used for experiments in early 2020 in Patras, Greece during the PyroTRACH-PANACEA Wintertime 2020

95   experiment. The system consists of two 1.5 m^3 Teflon (PTFE) reactors attached to metallic frames.

96   Use of the second reactor as a reference (control chamber) allows the identification and potential

97   correction for any major experimental artifacts that could be due to the walls of the chamber and

98   the other complexities of this experimental system. The dual chamber system was deployed from

99   January 10 till February 15, 2020 in the city of Patras. The chambers along with the available

100   instrumentation were located indoors, in the campus of the University of Peloponnese,

101   approximately a few kilometers away from the center of the city. The windows of the laboratory

102   were kept open before and during the experiments, so the temperature of the system was only a

103   few degrees higher than that of the outdoor environment.

104

105   **2.2 Experimental description**

106   Both chambers were flushed with ambient air before each experiment using a metal bellows

107   pump (Senior Aerospace, MB-602) for 1-2 h. This process is used to achieve higher sampling

108   efficiency and brings the system (chamber walls, tubing) close to equilibrium with ambient air

109   reducing losses of vapors to the sampling lines and walls of the chamber. Ambient air during

110   nighttime cold periods was introduced inside both chambers. In one of the chambers, (perturbed

111   chamber) ozone was added and upon reaction with the existing NO_x in the chamber formed NO_3

112   radicals. The second chamber (control chamber) was used as the reference in order to help us

113   understand the unperturbed evolution of the system inside the chamber. During all experiments

114   the chambers were under dark conditions. Ambient air was flushed through each of the chambers

115   with a flow of 80 L min^{-1}. More than 70% of the ambient PM was transferred to the chambers and

116   the concentrations of the measured VOCs were within 5% of their ambient values.

117   Using an automated valve switching between the two reactors, the particle and gas

118   concentrations in both chambers were measured. Data were collected 1.5 min after the switching

119   of the valve to avoid any memory effects related to the sampling lines. For the gas phase

120   measurements PTFE tubing (0.25 in) was used, while for the particle phase the tubing was copper

121   (0.25 in).

122   After filling the chambers with ambient air, the content of each chamber was characterized

123   for approximately one hour. The ozone added in the perturbed chamber after the characterization

124   period was in the range of 50-250 ppb. These values are higher than the 20 ppb measured during

125   the nighttime in Patras in this campaign, but some acceleration of the corresponding chemical

126 processes is necessary to reduce the effects of the walls and to limit the duration of the experiments

127 in the relatively small chambers used.

128 In selected experiments, approximately 40 ppb of d9-butanol was added in both chambers

129 to measure the OH concentration. Following Barnet et al. (2012), the OH concentration in the

130 chambers was estimated with the measured decay of the butanol concentration assuming a reaction

131 rate constant with OH of 3.4×10^{12} cm^3 molecule^{-1} s^{-1}.

132 An incoherent broad-band cavity-enhanced absorption spectroscopy (IBB-CEAS) was

133 used to measure the NO_3 radical concentration. Detailed information about the technique can be

134 found elsewhere (Venables et al., 2006; Ventrillard-Courtillot et al., 2010; Chen and Venables,

135 2011; Fouqueau et al., 2020). Briefly the light from a LED source centered on the 662 nm

136 absorption cross section of NO_3 radical is focused and introduced into a high-finesse optical cavity

137 composed of two high reflectivity (~99.98%) and 1 m curvature mirrors. The optical cavity has a

138 length of 0.61 m and allows up to 4.5 km (at 662 nm) optical path and a detection limit up to 3 ppt

139 (integration time of 10 seconds). Particle-free air is passed through the cavity at 2.5 L min^{-1}.

140 Spectra between 640 and 685 nm were recorded with an OceanOptics QE-65 Pro spectrometer. A

141 time resolution of one minute was selected for these experiments. Calibration with NO_2 (800 ppb

142 in dry nitrogen, Air Liquide) was performed daily in order to precisely determine the reflectivity

143 of the mirrors and estimate the optical path. The sample spectra were fitted against standard spectra

144 of gas species absorbing in the spectral region of the instrument: NO_3 radical (Orphal et al., 2003),

145 NO_2 (Vandaele et al., 1998) and H_2O (reference spectrum recorded with the instrument) using the

146 DOASIS software.

147 A quadrupole proton-transfer reaction mass spectrometer (PTR-MS, Ionicon Analytik) was

148 used to measure the concentration of VOCs including d9-butanol. We calculated the initial VOC

149 levels in the chambers using the concentrations of m/z 42 (acetonitrile), 69 (isoprene), 71 (MVK

150 & MACR), 73 (MEK), 79 (benzene), 93 (toluene) and 107 (xylene). We used the above m/z peaks,

151 because the PTR-MS was calibrated for those values. For the experiments that the PTR-MS was

152 not available we scaled the initial VOCs concentration using the BC levels. Using a series of gas

153 monitors the concentration of nitrogen oxides (NO and NO_2) and ozone (O_3) were measured

154 (Teledyne models: T201 and 400E respectively).

155 A TSI scanning mobility particle sizer (SMPS, classifier model 3080; DMA model 3081

156 CPC model 3775) was used for measuring the particle number distribution in the 15-700 nm range.

157   An Aerodyne high-resolution time-of-flight aerosol mass spectrometer (HR-ToF-AMS) was

158   measuring the composition and mass spectrum of OA. For the analysis of the HR-ToF-AMS data

159   we used the AMS software toolkit (SQUIRREL v1.57I) and for the high-resolution data the Peak

160   Integration by Key Analysis (PIKA v1.6I) software. The elemental ratios were calculated using

161   the improved method of Canagaratna et al. (2015). The mass concentration and particle distribution

162   of black carbon (BC) were measured using a single-particle soot photometer (SP2, Droplet

163   Measurement Techniques).

164   The collection efficiency (CE) of the AMS was calculated applying the algorithm of

165   Kostenidou et al. (2007), comparing the SMPS volume distributions and the AMS mass

166   distributions. The CE ranged between 0.40-0.45 depending on the experiment. Using the same

167   algorithm, the density of the OA was calculated to be in the range of 1.25-1.4 g cm^{-3}.

168   Using the theta (θ) angle (Kostenidou et al., 2009) a comparison between the OA spectra

169   of the ambient and the chamber content after filling, we concluded that the OA composition

170   injected in the chambers was the same as in the ambient air. The theta angle between the two

171   chambers and the ambient OA spectra was always less than 4 degrees, suggesting excellent

172   agreement. Also, the OA mass spectra in the two chambers right after their filling was in very good

173   agreement (θ=3-4°), confirming that both chambers had the same OA composition initially.

174   Following the completion of each perturbation experiment, a wall-loss characterization

175   experiment was conducted to measure the size-dependent particle wall-loss rate constant inside

176   the two chambers (Wang et al., 2018). The particles were produced by the atomization (TSI, model

177   3076) of an aqueous solution of ammonium sulfate (5 g L^{-1}) and subsequent diffusion drying and

178   were injected into both chambers. Using an ionizing fan, the chamber walls were swept before the

179   start of each experiment to keep the particle loss rates low (Jorga et al., 2020).

180   The perturbation experiments started around 18:00 LT each evening, when the OA

181   concentration was elevated from local nocturnal biomass burning emissions in the area for heating.

182   The initial conditions in the experiments are summarized in Table 1. Thirteen experiments, eleven

183   involving perturbation and two blank experiments, in which no ozone was injected in either

184   chamber, were performed during January and February 2020 using ambient air from Patras.

185

186

187

3 Results of a Typical Perturbation Experiment

188

189   The average PM_1 concentration in the chambers during the filling process of Exp. 1 was

190 approximately 50 μg m^{-3}. The concentration of OA during that period was 44 μg m^{-3} with 2.4 μg

191 m^{-3} of BC. The positive matrix factorization (PMF) analysis of the full campaign ambient data set

192 suggested that 70% of the OA at the time of filling originated from biomass burning. Other OA

193 sources included cooking OA (15%), oxygenated OA (10%) and hydrocarbon-like OA (5%). The

194 initial concentration of O_3 in the two chambers was 10 ppb, of NO 17 ppb and of NO_2 24 ppb,

195 values within 5% of their ambient concentrations. The measured initial VOC levels were

196 approximately 150 μg m^{-3}. The rest of the conditions are summarized in Table 1.

197   In Exp.1 NO_2 increased to 30 ppb in the perturbed chamber in approximately 30 min after

198 the ozone injection while at the same time NO levels dropped to close to zero. In the perturbed

199 chamber 2 hours after the injection the mixing ratio of NO_2 was 18 ppb and of ozone 220 ppb. In

200 the control chamber the concentrations of the above mentioned gases remained within 10% of their

201 initial levels. Due to the time needed for mixing and the rapid reaction of NO and O_3 it is difficult

202 to measure accurately the injected O_3 concentration. A zeroth order estimate can be made assuming

203 that the injected amount of ozone is equal to the final (equilibrated) amount of ozone in the

204 perturbed chamber plus the reacted NO_x (Table S1). Based on this zeroth order estimate, the

205 injected ozone in Exp. 1 was approximately 240 ppb.

206   Following the injection of ozone in the perturbed chamber (t=0 h) there was a rapid increase

207 of OA (Fig. 1). Approximately 33 μg m^{-3} of SOA was produced in 2.5 hours (70% increase from

208 the initial injected OA levels). In just one hour after the injection of ozone, the OA concentration

209 increased by approximately 25 μg m^{-3}. This roughly corresponds to an initial OA formation rate

210 of 25 μg m^{-3} h^{-1}, indicating the strong potential of the ambient air in an urban area with strong

211 biomass burning emissions to form SOA even under dark conditions. The change of OA in the

212 control chamber after the particle wall-loss corrections was less than 7% at all times. This strongly

213 indicates that the OA changes in the perturbation chamber were not due to experimental artifacts.

214   The sulfate concentration remained practically the same (within 10%) in both the perturbed

215 and the control chambers after accounting for particle wall-losses. The initial nitrate in the

216 perturbed chamber was 1 μg m^{-3} more than in the control. This small difference can be an artifact

217 of the sampling system in this specific experiment. Production of approximately 6 μg m^{-3} of aerosol

218 nitrate was observed in the perturbed chamber with the majority of this increase in the form of

219   organic nitrate. Using the method described in Farmer et al. (2010) using the NO^+/NO_2^+ ratio from

220   the AMS, we estimate that close to 60% of the formed secondary aerosol nitrate in the perturbed

221   chamber was organic. Taking into account the organic nitrate, there was a 77% increase of the OA

222   compared to the initial concentration.

223   An increase of the ammonium concentration by close to 1 $\mu g\ m^{-3}$ was observed in the

224   perturbed chamber while in the control its concentration remained within 8% of the initial value.

225   The relative humidity (RH) during Exp. 1 inside the chambers was approximately 45%.

226

227 3.1 Organic aerosol spectra

228   Comparing the OA mass spectra in the perturbed chamber at the beginning (after the air

229   injection) and at the end (2.5 hours after the ozone injection) of Exp. 1 there was an increase in the

230   fractional signal of m/z: 28 (CO^+), 29 (CHO^+), 30 (CH_2O^+), 43 ($C_2H_3O^+$), and 44 (CO_2^+). The

231   highest decrease was observed in 55 ($C_4H_7^+$), 57 ($C_4H_9^+$), 60 ($C_2H_4O_2^+$), 69 ($C_5H_9^+$), 91 ($C_7H_7^+$)

232   and 95 ($C_7H_{11}^+$). The theta angle between the spectra was 19 degrees, indicating significant change.

233   The initial and final spectra in the control chamber had a θ angle of 8 degrees, with changes in m/z

234   28, 44, 57 and 60. Figure 2 represents the OA mass spectra in the two chambers at the start and

235   end of Exp. 1.

236   The O:C ratio during Exp. 1 in the control chamber increased slightly from 0.4 to 0.41

237   during the experiment (Fig. 3). This suggests that there was relatively low but probably non-zero

238   chemical activity in this chamber. This is consistent with the small change in the OA mass

239   spectrum. This activity is probably due to the O_3 that existed in this chamber. On the contrary in

240   the perturbed chamber after the injection of ozone the O:C ratio increased rapidly reaching 0.52

241   after 30 min. At the end of the experiment, the O:C ratio in the perturbed chamber reached a value

242   of 0.61, similar to the measured ambient value around 3:00 LT at night.

243   To calculate the mass spectrum of the produced OA in the perturbed chamber, we used a

244   simple mass balance approach. Details about this method can be found in Jorga et al. (2020).

245   Concisely, assuming that the main processes in the chamber are losses of particles to the chamber

246   walls and SOA formation, we estimate the initial (before the injection of ozone) and produced OA

247   mass spectra. Using the particle rate loss constant measured at the end of each experiment, the

248   concentration of the preexisting OA as a function of time can be calculated. The produced OA is

249   then the difference between the total measured OA and the initial OA. Figure 4 shows the estimated

250   produced OA in Exp. 1 and Figure 5 the corresponding AMS spectrum.

251   The produced OA mass spectra from the perturbed chamber were compared with the

252   produced OA factor from dark aging of biomass burning emissions in the laboratory (Kodros et

253   al., 2020). Although the present study deals with ambient emissions with more complex air mixture

254   and conditions than the laboratory work that we are comparing with, that used specific biomass

255   burning emissions under idealized conditions, a comparison can provide us with information about

256   the consistency of the two studies. Kodros et al. (2020) performed chamber experiments in which

257   they exposed residential biomass burning emissions from a residential wood stove to NO_2 and O_3

258   under different RH conditions. Here we compare the produced OA from a medium RH

259   (approximately 45%) experiment with those of the ambient perturbation experiments that had

260   similar RH. The θ angle between the produced OA from perturbation Exp.1 and the one from the

261   laboratory chamber experiment was 11 degrees, indicating a considerable degree of similarity (Fig.

262   6).

263   The produced OA was also compared with the ambient oxygenated organic aerosol (OOA)

264   factor identified from the PMF analysis of the ambient data. The θ angle between the ambient

265   OOA in Patras from winter 2020 and the produced OA from Exp. 1 was 10 degrees. Similarities

266   were also observed in the produced OA and OOA from cities around the world during winter

267   periods. For Exp. 1 the θ angle was in the range of 9-18 degrees (Table S2) when compared with

268   OOA factors from Fresno, US (Ge et al., 2012), Barcelona, Spain (Mohr et al., 2012), Paris, France

269   (Crippa et al., 2013), Bologna, Italy (Gilardoni et al., 2016), Athens, Greece (Florou et al., 2017)

270   and Xi'an/Beijing, China (Elser et al., 2016).

271

272   4 Results of Other Experiments

273   4.1 Secondary organic aerosol production

274   The rapid OA production observed during Exp. 1 was also observed in all the other

275   experiments, with approximately 75% of the produced OA formed in the first hour after the ozone

276   injection. Figure 7 represents the produced OA (including organic nitrates) in all the perturbation

277   experiments. In all experiments, the majority of secondary nitrate aerosol were organonitrate,

278   representing 55-85% of the total produced nitrate. Taking into account the organic nitrates, the

279   initial OA formation rate in the perturbed chamber in the conducted experiments was on average

280   10 µg m^{-3} h^{-1} ranging from 1 to 30 µg m^{-3} h^{-1}.

281   An increase in the O:C in the perturbed chamber was observed in all experiments with an

282   average increase from the initial O:C of 45%. At the same time the O:C in the control chamber

283   remained within 6% of the initial value.

284   The mass spectra of the produced OA in the perturbed chamber were similar to that of

285   Exp.1 with the major m/z values being 28, 29, 43, 44, 55 and 69 (Fig. 5). The θ angle between the

286   different produced OA spectra in the perturbed experiments were less than 14 degrees, suggesting

287   similarities between the produced OA from the different perturbation experiments. The θ angle

288   between the produced OA mass spectra in the perturbed chamber and the one from Kodros et al.

289   (2020) was in the range of 9-16 degrees, suggesting similarity of the results of the two studies,

290   even if one relied on a single fuel burned in a single stove and the other in a mixture of emissions

291   from hundreds of fireplaces and heating stoves.

292

293   **4.2 NO₃ and OH radical levels**

294   Based on the decay of d9-butanol after the injection of ozone, the OH concentration was

295   in the range of 0.2-0.4×10^6 molecules cm^{-3} in the perturbation chamber suggesting that the addition

296   of ozone and reactions with organic vapors were not producing significant OH levels. In the control

297   chamber the corresponding OH concentrations were practically zero.

298   Nitrate radical concentrations above the detection level of a few ppt were only measured

299   in the perturbed chamber after the ozone injection. The maximum NO₃ radical concentrations in

300   the perturbed chamber ranged from 3 to 25 ppt with the highest observed during Exp. 8 (Table

301   S3). In this experiment before the ozone injection the NO₃ levels in both chambers were below the

302   detection limit of the instrument, while after the injection (t=0 h) the concentration of NO₃ started

303   to increase (Fig. S1). In Exp. 8 there were 44 ppb of NO$_x$ initially and 150 ppb of O₃ were injected.

304   Approximately 15 µg m^{-3} of OA was formed in 2.5 h after the perturbation, with close to 2 µg m^{-3}

305   of the OA formed being organic nitrate. The O:C reached a value of 0.6 at the end of this

306   experiment.

307   The measured NO₃ concentrations along with the low concentrations of OH in the

308   perturbed chamber suggests that the reactions of VOCs with NO₃ radicals and potentially ozone

309   were the major source of SOA production.

4.3 Factors affecting the SOA production

The highest produced SOA was observed, as expected, in experiments that had high initial OA and VOC levels and therefore took place during polluted conditions. Experiments 1, 4 and 6 had the highest measured inital VOC levels among the conducted experiments, close to 150 μg m^{-3} (Fig. S2). Although, only a fraction of the VOCs present in the atmosphere were measured by the PTR-MS in this work, these measurements provide an indication of the SOA formation potential of the corresponding air masses.

The absolute concentration of SOA formed was also affected by the levels of NO present. Experiments with low initial NO, less than 5 ppb, (Experiments 2, 3, 5 ,9 and 11) had the lowest SOA production. The lowest NO_3 radical concentrations were also observed in those experiments. Figure 8 shows the correlation between the concentration of NO_3 radicals and the produced organic nitrate levels in the perturbed chamber. The good correlation (R^2=0.79) supports the strong link between the NO_3 chemistry occurring in the perturbed chamber and the corresponding SOA production. This suggests that the oxidants levels (mainly NO_3) produced after reactions of ozone with the pre-existing NO_x are affecting significantly the levels of SOA formed under these conditions.

5 Conclusions

In this work, we studied the nighttime aging of urban wintertime air, strongly influenced by biomass burning emissions in Patras, Greece. Using a dual chamber system and ambient air as a starting point, we injected additional ozone in only one chamber to accelerate nitrate radical production via reactions with the pre-existing NO_x. The other chamber was used as a reference mainly as a safeguard against potential experimental artifacts.

After the addition of ozone, rapid SOA formation was observed in the perturbed chamber with the additional OA formed reaching up to 35 μg m^{-3}. The SOA formed increased the pre-existing OA by 20-70%. Most of the secondary nitrate formed was attributed to organics, in some cases reaching up to 85% of the total aerosol nitrate. The organic aerosol formation was rapid, with 75% of the produced OA formed in the first hour after the ozone injection. The organic aerosol content in the control chamber remained within 10% of the initial injected levels, suggesting limited chemical oxidation without the addition of ozone in these timescales.

340   The O:C of organic aerosol increased rapidly in the perturbed chamber following the ozone

341   injection. In 2-3 h of reactions a 40-50% increase of the O:C was observed while the OA O:C in

342   the control chamber remained within approximately 5% of the initial value. The produced OA

343   mass spectra showed similarities with the produced OA factor from a previous dark aging biomass

344   burning experiments under laboratory conditions. Furthermore, the produced SOA mass spectra

345   were quite similar to those of ambient oxygenated OA factors found in urban areas during winter

346   periods.

347   Nitrate radicals were observed only in the perturbed chamber and only after the ozone

348   injection. Their levels reached up to 25 ppt. Along with the low levels of hydroxyl radical in the

349   perturbed chamber, indicates that reaction with nitrate radicals and ozone were responsible for the

350   SOA formation and the change in the OA composition.

351

352   *Author Contribution*: S.D.J., K.F., C.K., J.K.K. and C.V. conducted the experiments, collected and

353   analyzed the data. S.N.P and A.N. conceived and directed the study. M.C., A.F. and B.P.-V.

354   provided the IBB-CEAS. S.D.J. and S.N.P. wrote the manuscript with inputs from all co-authors.

355

356   *Data availability*: Data related to this article are available upon request to the corresponding author.

357   The data will be available in the EUROCHAMP-2020 website.

358

359   *Competing interests*: The authors declare that they have no conflict of interest.

360

361   **Acknowledgements**

362   This work was supported by the European Union's Horizon 2020 EUROCHAMP–2020

363   Infrastructure Activity (grant agreement 730997) and project PyroTRACH (ERC-2016-COG)

364   funded from H2020-EU.1.1. - Excellent Science - European Research Council (ERC), project ID

365   726165. We thank Prof. A. Papalou and the University of Peloponnese for providing the space for

366   our experiments.

367

368   **References**

369   Ahern, A. T., Robinson, E. S., Tkacik, D. S., Saleh, R., Hatch, L. E., Barsanti, K. C., Stockwell,

370   C. E., Yokelson, R. J., Presto, A. A., Robinson, A. L., Sullivan, R. C. and Donahue, N. M.:

Production of secondary organic aerosol during aging of biomass burning smoke from fresh fuels and its relationship to VOC precursors, J. Geophys. Res., 124, 3583–3606, 2019.

Akagi, S. K., Yokelson, R. J., Wiedinmyer, C., Alvarado, M. J., Reid, J. S., Karl, T., Crounse, J. D. and Wennberg, P. O.: Emission factors for open and domestic biomass burning for use in atmospheric models, Atmos. Chem. Phys., 11, 4039–4072, 2011.

Akherati, A., He, Y., Coggon, M. M., Koss, A. R., Hodshire, A. L., Sekimoto, K., Warneke, C., De Gouw, J., Yee, L., Seinfeld, J. H., Onasch, T. B., Herndon, S. C., Knighton, W. B., Cappa, C. D., Kleeman, M. J., Lim, C. Y., Kroll, J. H., Pierce, J. R. and Jathar, S. H.: Oxygenated aromatic compounds are important precursors of secondary organic aerosol in biomass-burning emissions, Environ. Sci. Technol., 54, 8568–8579, 2020.

Alfarra, M. R., Prevot, A. S. H., Szidat, S., Sandradewi, J., Weimer, S., Lanz, V. A., Schreiber, D., Mohr, M. and Baltensperger, U.: Identification of the mass spectral signature of organic aerosols from wood burning emissions, Environ. Sci. Technol., 41, 5770–5777, 2007.

Andreae, M. O. and Merlet, P.: Emission of trace gases and aerosols from biomass burning, Global Biogeochem. Cycles, 15, 955–966, 2001.

Bond, T. C., Streets, D. G., Yarber, K. F., Nelson, S. M., Woo, J. H. and Klimont, Z.: A technology-based global inventory of black and organic carbon emissions from combustion, J. Geophys. Res., 109, D14203, doi:10.1029/2003JD003697, 2004.

Bougiatioti, A., Stavroulas, I., Kostenidou, E., Zarmpas, P., Theodosi, C., Kouvarakis, G., Canonaco, F., Prévôt, A. S. H., Nenes, A., Pandis, S. N. and Mihalopoulos, N.: Processing of biomass-burning aerosol in the eastern Mediterranean during summertime, Atmos. Chem. Phys., 14, 4793–4807, 2014.

Boy, J., Rollenbeck, R., Valarezo, C. and Wilcke, W.: Amazonian biomass burning-derived acid and nutrient deposition in the north Andean montane forest of Ecuador, Global Biogeochem. Cycles, 22, GB4011, 2008.

Brown, S. S., deGouw, J. A., Warneke, C., Ryerson, T. B., Dubé, W. P., Atlas, E., Weber, R. J., Peltier, R. E., Neuman, J. A., Roberts, J. M., Swanson, A., Flocke, F., McKeen, S. A., Brioude, J., Sommariva, R., Trainer, M., Fehsenfeld, F. C., and Ravishankara, A. R.: Nocturnal isoprene oxidation over the Northeast United States in summer and its impact on reactive nitrogen partitioning and secondary organic aerosol, Atmos. Chem. Phys., 9, 3027–3042, 2009

402 Brown, S. S., Dubé, W. P., Bahreini, R., Middlebrook, A. M., Brock, C. A., Warneke, C., de Gouw,
403   J. A., Washenfelder, R. A., Atlas, E., Peischl, J., Ryerson, T. B., Holloway, J. S., Schwarz,
404   J. P., Spackman, R., Trainer, M., Parrish, D. D., Fehshenfeld, F. C., and Ravishankara, A.
405   R.: Biogenic VOC oxidation and organic aerosol formation in an urban nocturnal boundary
406   layer: aircraft vertical profiles in Houston, TX, Atmos. Chem. Phys., 13, 11317–11337,
407   2013.

408 Bruns, E. A., El Haddad, I., Slowik, J. G., Kilic, D., Klein, F., Baltensperger, U. and Prévôt, A. S.
409   H.: Identification of significant precursor gases of secondary organic aerosols from
410   residential wood combustion, Sci. Rep., 6, 27881, 2016.

411 Canagaratna, M. R., Jimenez, J. L., Kroll, J. H., Chen, Q., Kessler, S. H., Massoli, P., Hildebrandt
412   Ruiz, L., Fortner, E., Williams, L. R., Wilson, K. R., Surratt, J. D., Donahue, N. M., Jayne,
413   J. T. and Worsnop, D. R.: Elemental ratio measurements of organic compounds using
414   aerosol mass spectrometry: characterization, improved calibration, and implications,
415   Atmos. Chem. Phys., 15, 253–272, 2015.

416 Capes, G., Johnson, B., McFiggans, G., Williams, P. I., Haywood, J. and Coe, H.: Aging of
417   biomass burning aerosols over West Africa: Aircraft measurements of chemical
418   composition, microphysical properties, and emission ratios, J. Geophys. Res., 113, 1–13,
419   2008.

420 Crippa, M., DeCarlo, P. F., Slowik, J. G., Mohr, C., Heringa, M. F., Chirico, R., Poulain, L.,
421   Freutel, F., Sciare, J., Cozic, J., Di Marco, C. F., Elsasser, M., Nicolas, J. B., Marchand,
422   N., Abidi, E., Wiedensohler, A., Drewnick, F., Schneider, J., Borrmann, S., Nemitz, E.,
423   Zimmermann, R., Jaffrezo, J.-L., Prévôt, A. S. H. and Baltensperger, U.: Wintertime
424   aerosol chemical composition and source apportionment of the organic fraction in the
425   metropolitan area of Paris, Atmos. Chem. Phys., 13, 961–981, 2013.

426 Decker, Z. C. J., Zarzana, K. J., Coggon, M., Min, K. E., Pollack, I., Ryerson, T. B., Peischl, J.,
427   Edwards, P., Dubé, W. P., Markovic, M. Z., Roberts, J. M., Veres, P. R., Graus, M.,
428   Warneke, C., De Gouw, J., Hatch, L. E., Barsanti, K. C. and Brown, S. S.: Nighttime
429   chemical transformation in biomass burning plumes: A box model analysis initialized with
430   aircraft observations, Environ. Sci. Technol., 53, 2529–2538, 2019.

431 Elser, M., Huang, R.-J., Wolf, R., Slowik, J. G., Wang, Q., Canonaco, F., Li, G., Bozzetti, C.,
432   Daellenbach, K. R., Huang, Y., Zhang, R., Li, Z., Cao, J., Baltensperger, U., El-Haddad, I.

433   and Prévôt, A. S. H.: New insights into PM$_{2.5}$ chemical composition and sources in two
434   major cities in China during extreme haze events using aerosol mass spectrometry, Atmos.
435   Chem. Phys., 16, 3207–3225, 2016.

436 Farmer, D. K., Matsunaga, A., Docherty, K. S., Surratt, J. D., Seinfeld, J. H., Ziemann, P. J. and
437   Jimenez, J. L.: Response of an aerosol mass spectrometer to organonitrates and
438   organosulfates and implications for atmospheric chemistry, Proc. Natl. Acad. Sci.., 107,
439   6670–6675, 2010.

440 Favez, O., El Haddad, I., Piot, C., Boréave, A., Abidi, E., Marchand, N., Jaffrezo, J.-L., Besombes,
441   J.-L., Personnaz, M.-B., Sciare, J., Wortham, H., George, C. and D'Anna, B.: Inter-
442   comparison of source apportionment models for the estimation of wood burning aerosols
443   during wintertime in an Alpine city (Grenoble, France), Atmos. Chem. Phys., 10, 5295–
444   5314, 2010.

445 Florou, K., Papanastasiou, D. K., Louvaris, E., Kaltsonoudis, C., Patoulias, D., Pikridas, M.,
446   Gkatzelis, G. I., Pandis, S. N. and Mihalopoulos, N.: The contribution of wood burning and
447   other pollution sources to wintertime organic aerosol levels in two Greek cities, Atmos.
448   Chem. Phys., 17, 3145–3163, 2017.

449 Ford, B., Val Martin, M., Zelasky, S. E., Fischer, E. V., Anenberg, S. C., Heald, C. L. and Pierce,
450   J. R.: Future fire impacts on smoke concentrations, visibility, and health in the contiguous
451   United States, GeoHealth, 2, 229–247, 2018.

452 Fouqueau, A., Cirtog, M., Cazaunau, M., Pangui, E., Zapf, P., Siour, G., Landsheere, X., Méjean,
453   G., Romanini, D., and Picquet-Varrault, B.: Implementation of an incoherent broadband
454   cavity-enhanced absorption spectroscopy technique in an atmospheric simulation chamber
455   for in situ NO3 monitoring: characterization and validation for kinetic studies, Atmos.
456   Meas. Tech., 13, 6311–6323, 2020.

457 Fountoukis, C., Megaritis, A. G., Skyllakou, K., Charalampidis, P. E., Denier van der Gon, H. A.
458   C., Crippa, M., Prévôt, A. S. H., Fachinger, F., Wiedensohler, A., Pilinis, C. and Pandis, S.
459   N.: Simulating the formation of carbonaceous aerosol in a European Megacity (Paris)
460   during the MEGAPOLI summer and winter campaigns, Atmos. Chem. Phys., 16, 3727–
461   3741, 2016.

462 Fuller, G. W., Tremper, A. H., Baker, T. D., Yttri, K. E. and Butterfield, D.: Contribution of wood
463   burning to PM10 in London, Atmos. Environ., 87, 87–94, 2014.

464   Ge, X., Setyan, A., Sun, Y. and Zhang, Q.: Primary and secondary organic aerosols in Fresno,
465   California during wintertime: Results from high resolution aerosol mass spectrometry, J.
466   Geophys. Res., 117, D19301, doi:10.1029/2012JD018026, 2012.

467   Gilardoni, S., Massoli, P., Paglione, M., Giulianelli, L., Carbone, C., Rinaldi, M., Decesari, S.,
468   Sandrini, S., Costabile, F., Gobbi, G. P., Pietrogrande, M. C., Visentin, M., Scotto, F.,
469   Fuzzi, S. and Facchini, M. C.: Direct observation of aqueous secondary organic aerosol
470   from biomass-burning emissions, Proc. Natl. Acad. Sci., 113, 10013–10018, 2016.

471   Hartikainen, A., Yli-Pirilä, P., Tiitta, P., Leskinen, A., Kortelainen, M., Orasche, J., Schnelle-
472   Kreis, J., Lehtinen, K. E. J., Zimmermann, R., Jokiniemi, J. and Sippula, O.: Volatile
473   organic compounds from logwood combustion: Emissions and transformation under dark
474   and photochemical aging conditions in a smog chamber, Environ. Sci. Technol., 52, 4979–
475   4988, 2018.

476   Hennigan, C. J., Miracolo, M. A., Engelhart, G. J., May, A. A., Presto, A. A., Lee, T., Sullivan, A.
477   P., McMeeking, G. R., Coe, H., Wold, C. E., Hao, W.-M., Gilman, J. B., Kuster, W. C., de
478   Gouw, J., Schichtel, B. A., Collett, J. L., Kreidenweis, S. M. and Robinson, A. L.: Chemical
479   and physical transformations of organic aerosol from the photo-oxidation of open biomass
480   burning emissions in an environmental chamber, Atmos. Chem. Phys., 11, 7669–7686,
481   2011.

482   Jolleys, M. D., Coe, H., McFiggans, G., Taylor, J. W., O'Shea, S. J., Le Breton, M., Bauguitte, S.
483   J.-B., Moller, S., Di Carlo, P., Aruffo, E., Palmer, P. I., Lee, J. D., Percival, C. J. and
484   Gallagher, M. W.: Properties and evolution of biomass burning organic aerosol from
485   Canadian boreal forest fires, Atmos. Chem. Phys., 15, 3077–3095, 2015.

486   Jorga, S. D., Kaltsonoudis, C., Liangou, A. and Pandis, S. N.: Measurement of formation rates of
487   secondary aerosol in the ambient urban atmosphere using a dual smog chamber system,
488   Environ. Sci. Technol., 54, 1336–1343, 2020.

489   Kaltsonoudis, C., Jorga, S. D., Louvaris, E., Florou, K. and Pandis, S. N.: A portable dual-smog-
490   chamber system for atmospheric aerosol field studies, Atmos. Meas. Tech., 12, 2733–2743,
491   2019.

492   Kodros, J. K., Papanastasiou, D. K., Paglione, M., Masiol, M., Squizzato, S., Florou, K.,
493   Skyllakou, K., Kaltsonoudis, C., Nenes, A. and Pandis, S. N.: Rapid dark aging of biomass

494   burning as an overlooked source of oxidized organic aerosol, Proc. Natl. Acad. Sci., 52,
495   33028-33033, 2020.

496 Kostenidou, E., Pathak, R. K. and Pandis, S. N.: An algorithm for the calculation of secondary
497   organic aerosol density combining AMS and SMPS data, Aerosol Sci. Technol., 41, 1002–
498   1010, 2007.

499 Kostenidou, E., Lee, B. H., Engelhart, G. J., Pierce, J. R. and Pandis, S. N.: Mass spectra
500   deconvolution of low, medium, and high volatility biogenic secondary organic aerosol,
501   Environ. Sci. Technol., 43, 4884–4889, 2009.

502 Mohr, C., DeCarlo, P. F., Heringa, M. F., Chirico, R., Slowik, J. G., Richter, R., Reche, C.,
503   Alastuey, A., Querol, X., Seco, R., Peñuelas, J., Jiḿenez, J. L., Crippa, M., Zimmermann,
504   R., Baltensperger, U. and Prév̂ot, A. S. H.: Identification and quantification of organic
505   aerosol from cooking and other sources in Barcelona using aerosol mass spectrometer data,
506   Atmos. Chem. Phys., 12, 1649–1665, 2012.

507 O'Dell, K., Ford, B., Fischer, E. V. and Pierce, J. R.: Contribution of Wildland-Fire Smoke to US
508   PM 2.5 and Its Influence on Recent Trends, Environ. Sci. Technol., 53, 1797–1804, 2019.

509 Orphal, J., Fellows, C. E., and Flaud, P.-M.: The visible absorption spectrum of NO_3 measured by
510   high-resolution Fourier transform spectroscopy, J. Geophys. Res., 108, 4077,
511   doi:10.1029/2002JD002489, 2003.

512 Ortega, A. M., Day, D. A., Cubison, M. J., Brune, W. H., Bon, D., De Gouw, J. A. and Jimenez,
513   J. L.: Secondary organic aerosol formation and primary organic aerosol oxidation from
514   biomass-burning smoke in a flow reactor during FLAME-3, Atmos. Chem. Phys., 13,
515   11551–11571, 2013.

516 Robinson, A. L., Subramanian, R., Donahue, N. M., Bernardo-Bricker, A. and Rogge, W. F.:
517   Source apportionment of molecular markers and organic aerosol. 2. Biomass smoke,
518   Environ. Sci. Technol., 40, 7811–7819, 2006.

519 Sundarambal, P., Balasubramanian, R., Tkalich, P. and He, J.: Impact of biomass burning on
520   Ocean water quality in Southeast Asia through atmospheric deposition: Field observations,
521   Atmos. Chem. Phys., 10, 11323–11336, 2010.

522 Tkacik, D. S., Robinson, E. S., Ahern, A., Saleh, R., Stockwell, C., Veres, P., Simpson, I. J.,
523   Meinardi, S., Blake, D. R., Yokelson, R. J., Presto, A. A., Sullivan, R. C., Donahue, N. M.
524   and Robinson, A. L.: A dual-chamber method for quantifying the effects of atmospheric

525   perturbations on secondary organic aerosol formation from biomass burning emissions, J.
526   Geophys. Res., 122, 6043–6058, 2017.

527 Tsimpidi, A. P., Karydis, V. A., Pozzer, A., Pandis, S. N. and Lelieveld, J.: ORACLE (v1.0):
528   module to simulate the organic aerosol composition and evolution in the atmosphere,
529   Geosci. Model Dev., 7, 3153–3172, 2014.

530 Vakkari, V., Beukes, J. P., Dal Maso, M., Aurela, M., Josipovic, M. and van Zyl, P. G.: Major
531   secondary aerosol formation in southern African open biomass burning plumes, Nat.
532   Geosci., 11, 580–583, 2018.

533 Vandaele, A. C., Hermans, C., Simon, P. C., Carleer, M., Colin, R., Fally, S., Mérienne, M. F.,
534   Jenouvrier, A., and Coquart, B.: Measurements of the NO_2 absorption cross-section from
535   42 000 cm^{-1} to 10 000 cm^{-1} (238–1000 nm) at 220K and 294 K., J. Quant. Spectrosc. Radiat.
536   Transf., 59, 171–184, 1998.

537 Wang, N., Jorga, S. D., Pierce, J. R., Donahue, N. M. and Pandis, S. N.: Particle wall-loss
538   correction methods in smog chamber experiments, Atmos. Meas. Tech., 11, 6577–6588,
539   2018.

540 Watson, J. G.: Visibility: Science and regulation, J. Air Waste Manag. Assoc., 52, 628–713, 2002.

541 Yu, J., Cocker, D. R., Griffin, R. J., Flagan, R. C. and Seinfeld, J. H.: Gas-phase ozone oxidation
542   of monoterpenes: Gaseous and particulate products, J. Atmos. Chem., 34, 207–258, 1999.

543 Zhao, D. F., Kaminski, M., Schlag, P., Fuchs, H., Acir, I.-H., Bohn, B., Häseler, R., Kiendler-
544   Scharr, A., Rohrer, F., Tillmann, R., Wang, M. J., Wegener, R., Wildt, J., Wahner, A. and
545   Mentel, T. F.: Secondary organic aerosol formation from hydroxyl radical oxidation and
546   ozonolysis of monoterpenes, Atmos. Chem. Phys., 15, 991–1012, 2015.

547

548

549

550

551

552

553

554

555

556   **Table 1:** Initial conditions for the dual chamber experiments.

Exp.	Start Time (LT)	RH (%)	Temperature (°C)	BC ($\mu g\ m^{-3}$)	OA ($\mu g\ m^{-3}$)	O:C	NO (ppb)	NO$_2$ (ppb)
1	17:45	45	17	2.4	44	0.4	17	24
2	17:45	35	13	0.8	18	0.36	4	22
3	17:50	33	15	0.6	19	0.25	3	20
4	17:55	40	14	2.5	48	0.33	90	20
5	17:45	35	15	1.1	18	0.4	3	25
6	17:50	40	17	2.6	50	0.36	32	25
7	18:00	45	20	1.0	16	0.36	15	20
8	17:55	42	22	1.2	22	0.45	22	22
9	18:15	40	19	0.7	16	0.44	3	14
10	18:15	45	21	1.6	25	0.33	32	21
11	18:30	45	24	0.6	6	0.41	1	5
12[a]	18:00	32	21	2.1	6	0.37	3	15
13[a]	18:20	30	19	3.0	33	0.35	31	23

557
558   [a] Blank experiments.
559

560

561

562

563

564

565
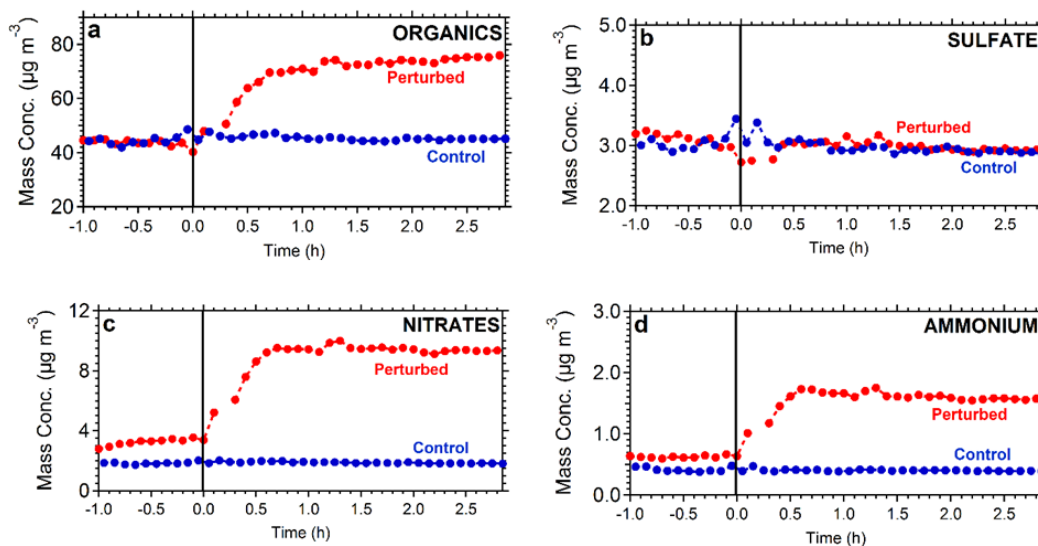
566

567

568 **Figure 1:** Particle wall-loss corrected aerosol mass concentration (CE=0.4) for the AMS-measured

569 (a) organics, (b) sulfate, (c) nitrates, and (d) ammonium in both the perturbed (red line) and the

570 control chamber (blue line) during Exp. 1.

571

572

573

574

575

576

577

578

579

580

581

582

583

584

585
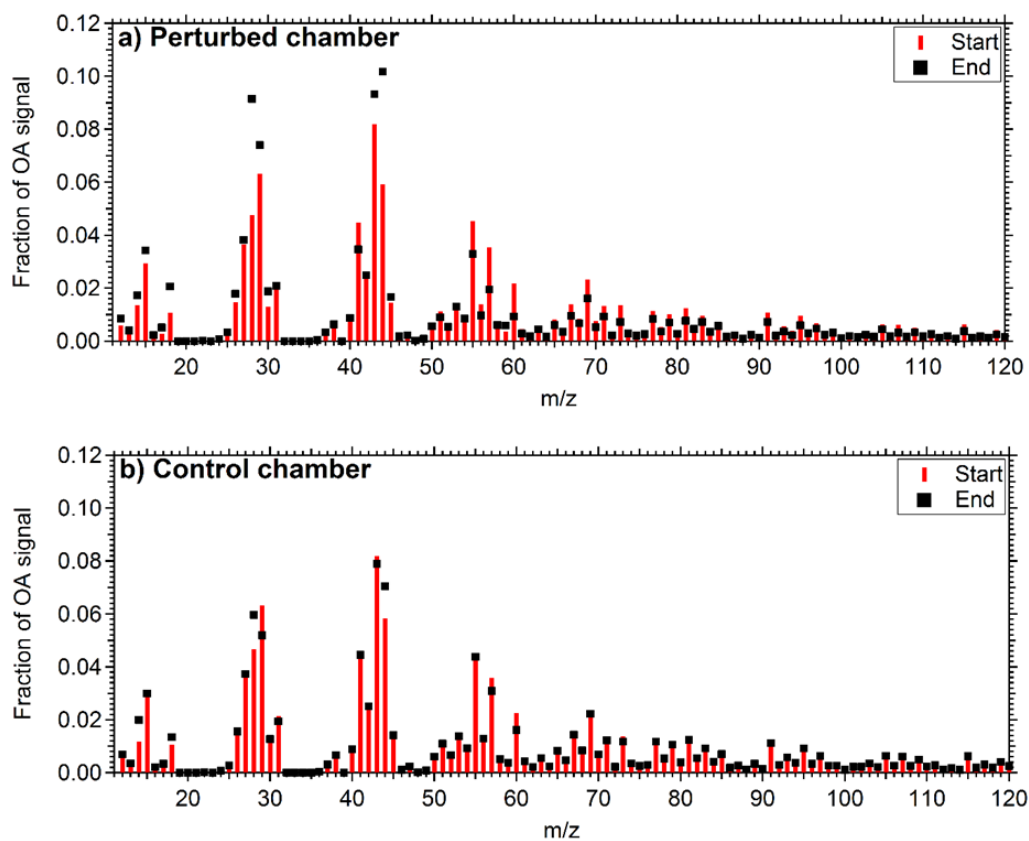
586
587
588 **Figure 2:** Mass spectra of OA during Exp. 1 in the (a) perturbed chamber and (b) control chamber
589 at the start of the experiment (after the filling process) and at the end of the experiment.
590
591
592

593
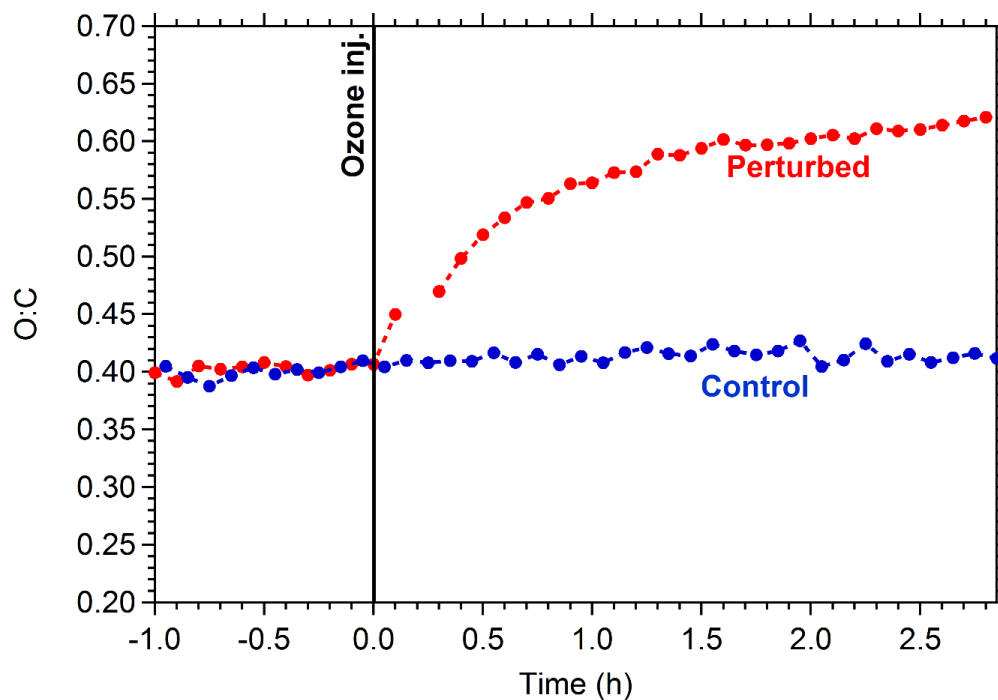
594 **Figure 3:** Oxygen to carbon ratio of the OA in the perturbed (red line) and the control chamber

595 (blue line) during Exp. 1.

596

597

598

599

600

601

602

603

604

605

606

607

608
609
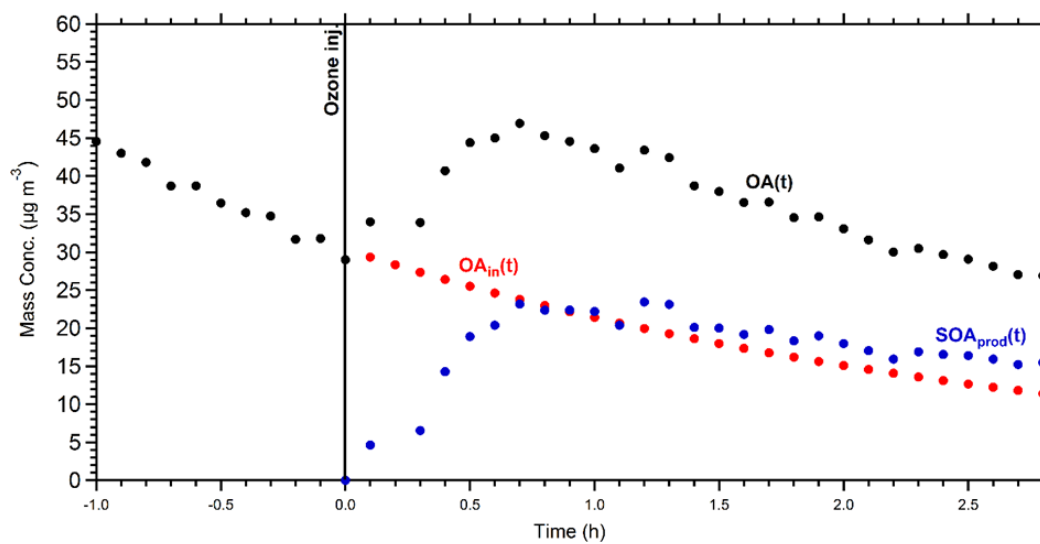
Figure 4: Mass concentration of the measured OA (black points), the initial OA (red points) and the produced SOA (blue points) in the perturbed chamber in Exp. 1. All concentrations refer to the suspended aerosol in the chamber and do not include the material deposited on the chamber walls.

613
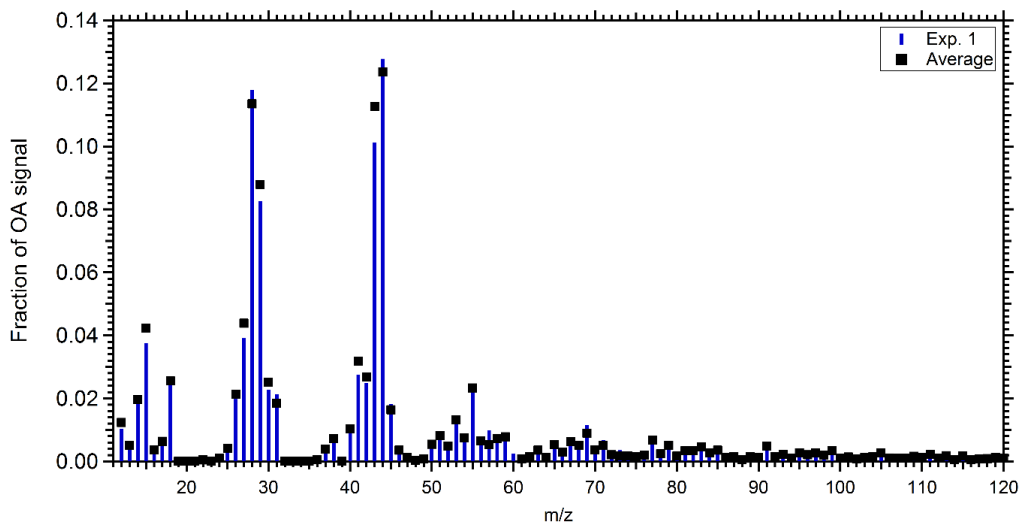
Figure 5: Mass spectrum of the produced SOA in the perturbed chamber for Exp. 1 (blue bars)

and the average spectrum of the produced SOA in all experiments (black squares).

616

617

618

619

620

621

622

623

624

625

626

627

628

629

630

631

632

633
634
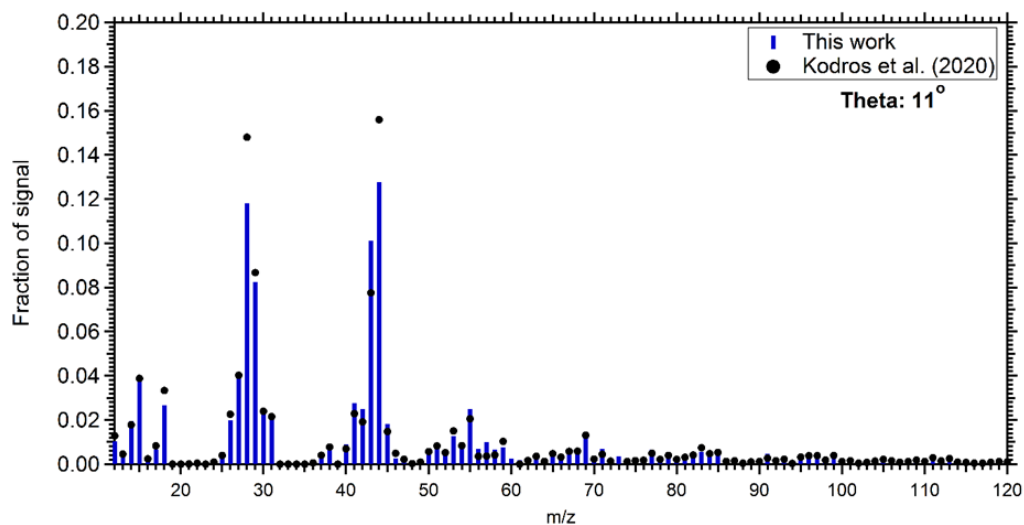
Figure 6: Comparison of the produced SOA mass spectra in the perturbed chamber during Exp. 1
(blue bars) and the produced SOA estimated during the chamber experiments of nocturnal aging
of biomass burning emissions (Kodros et al. 2020) (black circles).

638
639
640
641
642
643
644
645
646
647
648
649
650
651
652
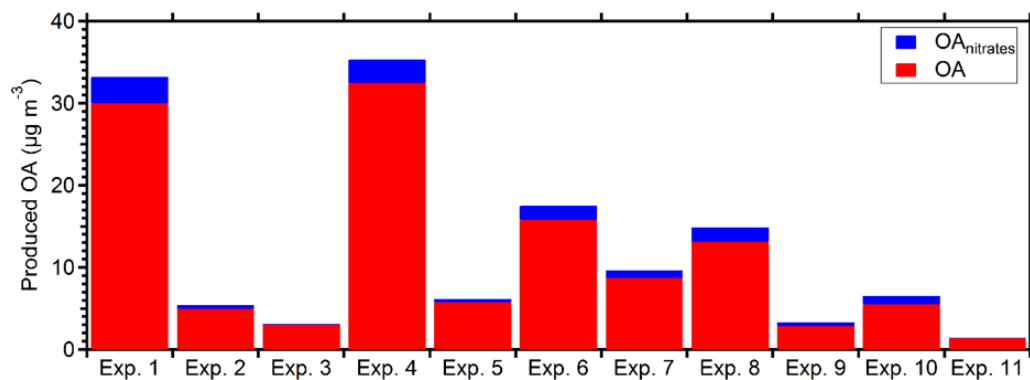
Figure 7: Produced OA (red bars) and the estimated organic nitrate (blue bars) in the perturbed chamber for the eleven perturbation experiments. All values have been corrected for wall losses and the AMS collection efficiency.

675
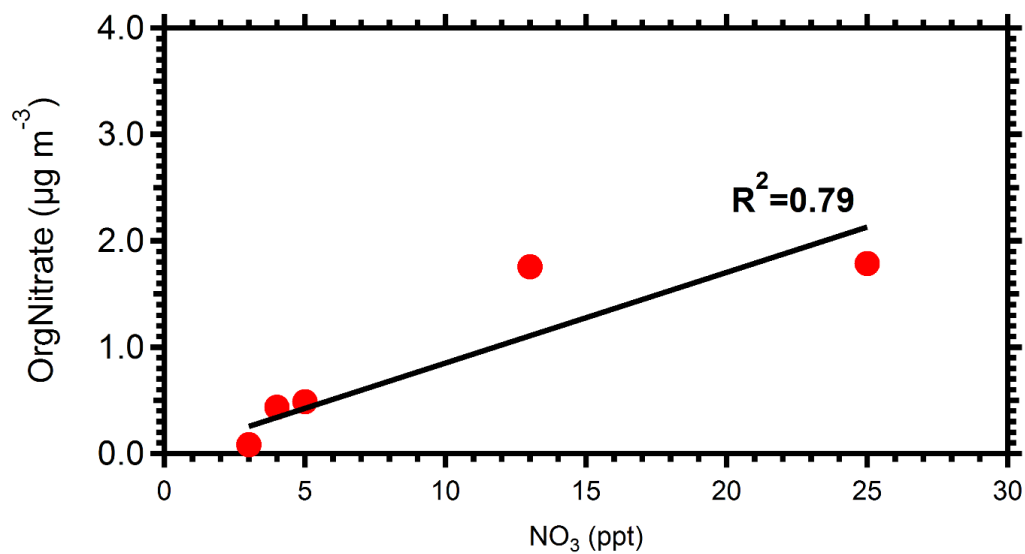
676 **Figure 8**: Correlation between NO_3 radicals with the organic nitrate formed in the perturbed

677 chamber.

678

679

680

681